Mixed Transition Metal Titanate and Vanadate Negative Electrode Materials for Na-ion Batteries

Z. L. Brown, S. Smith and M. N. Obrovac*

Department of Chemistry, Dalhousie University, Halifax, N.S., B3H 4R2 Canada

* - corresponding author: mnobrovac@dal.ca

Abstract

Sodium-ion batteries have the potential to be a low cost, sustainable replacement for lithium-ion batteries in large scale energy storage. The lack of practical negative electrode materials limit the development of Na-ion batteries. In this study, mixed transition metal titanates and vanadates were synthesized and electrochemically characterized in Na cells as well as Li cells for comparison. Some of these materials were found to have volumetric capacities that far exceeded that of Li in graphite. $Co_3V_3O_8$, $CoTiO_3$ and $Ca_5Co_4(VO_4)_6$ were found to have sodiation mechanisms that were not simple conversion reactions. $CoTiO_3$ in particular had low hysteresis and good reversibility, which is suggestive of an intercalation mechanism.

Introduction

Lithium ion batteries are widely used today, and have been successfully employed in large stationary energy storage applications, and in electric vehicles.[1] However, growing concerns of the cost of this technology as well as its environmental sustainability have sparked interest in sodium-ion battery technology.[2,3] Specifically, similarities between Li and Na chemistry coupled with the low cost and high abundance of Na make Na-ion battery technology very attractive. The expectation is that because of these characteristics, high energy density batteries may be developed from Na-ion battery technology for commercialization.

The lack of practical high energy density negative electrode materials limits Na-ion battery development. Graphite is the most commonly used negative electrode material for Li batteries, having a low voltage and high theoretical capacity of 372 mAh/g or 750 Ah/L. However, Na does not intercalate into graphite to a significant degree.[4] Reversible sodiation has been demonstrated in hard carbon, but its density is low, resulting in a low volumetric capacity (~450 Ah/L).[5] This limits the use of hard carbon as a practical negative electrode material motivating researchers to pursue other chemistries.

Various metal oxide materials have shown promise as negative electrode candidates for Na-ion batteries as intercalation compounds. Specifically, titanium and vanadium oxides are of interest due to the low-voltage redox couples of $Ti^{3+/4+}$ and $V^{2+/3+}$. For example, the lowest voltage for any Na intercalation oxide compound studied is $Na_2Ti_3O_7$, with a reversible plateau around 0.3 V versus Na/Na^+ with a corresponding capacity of 200 mAh/g (~688 Ah/L)[6]. Other low voltage titanates have recently been demonstrated as well, such as Na reversible intercalation in the

vacancies in $Na_xNi_{x/2}Ti_{1-x/2}O_2$.[7,8] However, intercalation mechanisms have limited capacities due to the finite number of vacancies that Li or Na ions can occupy whereas the capacities in conversion reactions have the potential to be significantly larger.[9]

Conversion reactions in metal ion cells are those in which an active electrode material, MX_y, reacts with an alkali metal ion, A, via a displacement reaction, which may be represented by the general reaction:[10]

$$M_aX_b + (bc)A \leftrightarrow aM + bA_cX. \quad (1)$$

Conversion reactions have been well studied in Li-ion batteries for both binary transition metal oxides and mixed transition metal oxides.[11] Conversely, not many have been studied for Na-ion batteries. One example of a mixed transition metal oxide negative electrode candidate for Na-ion batteries is $NiCo_2O_4$ spinel, which has a reversible capacity of 884 mAh/g with Li (close to its theoretical capacity) and 200 mAh/g (~1196 Ah/L) with Na when cycled from 0 to 3 V.[12] Co and Ni metal appear to be formed in the products after full lithiation, suggesting a conversion mechanism is occurring. When nanosized, simple oxides such as, Fe_2O_3, Co_3O_4, Mn_3O_4 and NiO have been found to have significant capacity via conversion reactions with Na.[13] Specifically, nano-Fe_2O_3 undergoes a full reduction to Fe with a hysteresis between 0.75–1.0 V, a relatively low value for Na-ion conversion reactions.[13] As these capacities are comparable to hard carbon in Na-ion cells, the potential for high energy density negative electrode materials via conversion reactions deserves more attention.

A mechanism other than conversion has been suggested to describe the lithiation of vanadates at low voltage, where amorphization of the mixed transition vanadate is observed.[14,15,16,17] For

example, the abnormally large lithiation capacity of $VFeO_4$ may be attributed to the role of O as a reaction centre since full reduction of Fe^{3+} or V^{5+} to Fe or V metal, respectively, was not observed.[17] Another example is the low voltage lithiation of brannerite-structured MnV_2O_6, which resulted in a large initial discharge capacity of 1400 mAh/g, accompanied by irreversible amorphization.[16] This was subsequently followed by 800 mAh/g of reversible capacity upon cycling where the O anions are believed to be contributing to this capacity.[16] The undesirable voltage curve polarization associated with conversion reactions can also be attributed to the role of O in the redox process, as breaking strong Li-O bonds during delithiation requires a larger electrochemical potential compared to removing inserted Li from an open framework.[18] The success in obtaining large capacities with lithium encourages the investigation of the sodiation of mixed vanadates.

In this study, several mixed transition metal titanates and vanadates were synthesized and their electrochemistry as negative electrodes were investigated in Na and Li half-cells. Structural changes during sodiation were investigated by ex-situ and quasi in-situ X-ray diffraction. Low average voltage capacity was observed with unique voltage curves which are discussed.

Experimental

Preparation of Materials - Several first row transition metal titanates and vanadates were synthesized via ball milling then heating stoichiometric amounts of as-purchased precursor reagents shown in Table 1. Ball milling was conducted with a Spex mixer-mill (SPEX CertiPrep) in 64 mL hardened steel ball-mill vials with two 0.5 in. hardened steel balls. The mass of the combined precursors never exceeded 6.00 grams. Non stoichiometric amounts of precursors

were only used in the synthesis of $Ca_5Co_4(VO_4)_6$, where a 1:1:1 atomic ratio of CaO, CoO and V_2O_5 were used. The ball milled powders were then heated in a tube furnace according to the conditions listed in Table 1. Compounds synthesized under argon were immediately transferred to an argon filled glove box without air exposure.

X-ray Diffraction Measurements - Materials were characterized by X-ray powder diffraction (XRD) using a Rigaku Ultima IV X-Ray Diffractometer equipped with a Cu anode X-ray tube and dual detectors. A scintillation detector with a diffracted beam monochromator was used to measure XRD patterns of powder samples.

Electrochemical cell Assembly and Cycling - 2325 type coin cells were assembled to evaluate the electrochemical performance of electrode materials in Li and Na half-cells. Electrodes consisted of active material, carbon black (Super P, Erachem Europe), and PVDF (polyvinylidene fluoride, Kynar HSV 900) in an 8:1:1 weight ratio. These components were thoroughly mixed in N-methyl-2-pyrrolidone (Sigma Aldrich, anhydrous 99.5%) with two tungsten carbide balls in a Retsch PM200 rotary mill (100 rpm, 1 hour) to create a uniform black slurry. The slurry was then coated onto aluminum or copper foil and dried under vacuum at 120 °C for 2 hours. Electrodes with aluminum foil current collectors were used for Na cells only. Circular electrodes, 2 cm^2 in area, were punched from the resulting coatings. Coin cell preparation was carried out in an argon filled glove box. Li and Na foil disk anodes were punched from thin foil (0.015 inch) that was rolled from thick Li foil or a Na ingot, respectively (Sigma Aldrich, ACS reagent grade). The electrolyte was 1 M $NaPF_6$ (Sigma Aldrich 98%) dissolved in 1/2 ethylene carbonate/diethyl carbonate by volume, with 10% by mass monofluoroethylene carbonate (all

from Novolyte Technologies). Two Celgard 2300 and one BMF (blown microfiber separator, 3M Company) were used as separators. Cells were tested with a Maccor Series 4000 Automated Test System (Maccor Inc., Tulsa, Oklahoma). Most cells were cycled between 0.005 to 2.5 V and/or 0.005 to 4.3 V at constant currents of 15 mA/g with a trickle discharge to 7.5 mA/g. $TiVO_4$ and $MnTiO_3$ cells were cycled at constant currents of 3.75 mA/g with a trickle discharge to 1.875 mA/g. $CoTiO_3$ cells were cycled at constant currents of 17 mA/g with a trickle discharge to 8.5 mA/g.

Ex-situ X-ray diffraction measurements - Conflat cells (as described in Reference[19]) were constructed with the compounds $CoTiO_3$, $Ca_5Co_4(VO_4)_6$ and CoV_3O_8 were discharged under the same conditions as the coin cells described above. Electrodes were then carefully removed from the cells at different states of charge in an argon filled glove box. The coatings were scraped off the copper current collector and rinsed with dimethyl carbonate (Novolyte Technologies). The coating was then placed into a gas-tight sample stage under argon gas for XRD measurements. The stage has an arch shaped aluminized Mylar™ window that does not contribute to the XRD patterns (DPM Solutions).

Measurement of Volume Expansion – The thickness of four fresh $CoTiO_3$ electrodes were measured to within ± 1μm with a Mitutoyo 293-340 precision micrometer. These electrodes were sodiated by discharging in a Na half-cell under the conditions described above. Electrodes were then carefully removed from the cells in an argon-filled glove box and the electrode thicknesses were measured again. The coating volume was then determined by subtracting the thickness of

131 the Al current collector and multiplying by the coating area. The measured volumes of the initial
132 and sodiated $CoTiO_3$ electrodes were used to determine the volume expansion
133
134 *Preparation of quasi in-situ X-ray diffraction measurements* – $CoTiO_3$ was coated directly onto a
135 beryllium disk with the same slurry compositions as described above. The Be disk served as both
136 a current collector and as an X-ray window in a coin cell, so that XRD patterns could be obtained
137 of the working electrode. Roscobond (Rosco Laboratories Inc.), a water-based contact adhesive,
138 was used to affix the beryllium window to the inside of a coin cell can with circular hole cut in it.
139 The coin cell was then assembled in the same manner as described above. After it was crimped
140 shut, Torr Seal (Varian) was applied to the outside of the coin cell at the beryllium/coin cell can
141 junction to ensure that the coin cell was properly sealed.
142
143 A quasi *in-situ* procedure was used where the cell was cycled as described above, then paused at
144 appropriate voltages while XRD measurements were performed. The cycling procedure was
145 continued after each XRD measurement.
146
147 **Results and Discussion**
148 *Structural Identification* –The XRD patterns of the prepared samples are shown in Figure 1 with
149 the identifying Powder Diffraction File (PDF) number indicated.[20] Most materials were
150 identified to be phase pure. Exceptions are $Ca_5Co_4(VO_4)_6$, which had a minor $Co_3V_2O_8$ impurity,
151 and CoV_3O_8, $CrVO_4$, which had minor unidentified impurities.
152
153 *Electrochemical Studies* -

Figure 2 shows the voltage curves of all the materials studied vs. lithium and vs. sodium. The voltage curves of $VFeO_4$, $Co_2V_2O_7$, $Mn_2V_2O_7$, CoV_3O_8, and MnV_2O_6 vs. lithium have high first discharge lithiation capacities, large reversible capacities and large voltage curve polarization. These features are typical of materials that undergo conversion reactions. $Ca_5Co_4(VO_4)_6$ and $CoTiO_3$ have lower first lithiation capacities and lower polarization. Such features are atypical of conversion reactions, and will be discussed in detail later. Reversible sodiation occurs for $CoTiO_3$, $VFeO_4$, $Ca_5Co_4(VO_4)_6$, CoV_3O_8, and MnV_2O_6. In general the initial sodiation capacities are much less than the lithiation capacities for all materials and are just a fraction of the theoretical capacity. Thermodynamically these oxides should react completely with sodium to form reduced metals and sodium oxide. The low capacity observed is indicative that the complete conversion reaction is kinetically hindered. However, the lower voltage polarization for sodium cells seems to indicate that the reaction that occurs is less kinetically hindered than a typical conversion reaction. All other materials were essentially inactive towards sodiation at 30°C. $CrVO_4$ and $TiVO_4$ were inactive towards Li and Na.

Figure 3 shows the observed reversible capacities versus the theoretical capacities for all of the materials studied. These values are tabulated in Table 2. Excepting $VFeO_4$, all materials have observed capacities that are far below the theoretical capacity based on a full conversion reaction. This suggests that either the conversion reactions are incomplete or that lithiation/sodiation proceeds via a different mechanism. As mentioned above, most of the materials studied have significantly larger reversible lithiation capacities compared to their reversible sodiation capacities, with a fraction of the theoretical capacity achieved in sodium cells. $VFeO_4$ has the largest lithiation and sodiation capacities suggesting it is the most

electrochemically active material studied. The compounds containing Co consistently have more sodiation capacity than Mn compounds, even when comparing isostructural $CoTiO_3$ and $MnTiO_3$. It is not clear why this should be the case. Although the reversible sodiation capacities are generally much smaller than that of Li, the volumetric sodiation capacities for some compounds are nevertheless quite high. In fact MnV_2O_6, CoV_3O_8, and $VFeO_4$ (820 - 1163 Ah/L) all have reversible volumetric sodiation capacities that far exceed that of hard carbon (~450 Ah/L) and even that of graphite in a lithium ion cell (~730 Ah/L).

Figure 4 shows the average polarization between the first charge and second discharge for the lithiation and sodiation for materials with significant reversible sodiation capacity, *i.e.* $CoTiO_3$, $VFeO_4$, $Ca_5Co_4(VO_4)_6$, CoV_3O_8, and MnV_2O_6. $Ca_5Co_4(VO_4)_6$ and $VFeO_4$ have the lowest voltage polarization in sodium cells, and $Ca_5Co_4(VO_4)_6$ also has the lowest polarization in lithium cells. In general the polarization values are similar to that of nanosized oxides with relatively low polarization, such as nano-Fe_2O_3 (0.75 – 1.0 V)[13], suggesting conversion mechanisms are possible in these reactions. However, this polarization reduces significantly during cycling in the case of $CoTiO_3$, as will be shown below.

Figure 5(a) shows the 2nd cycle and 50th cycle of $CoTiO_3$ vs. Na. During the second charge, 128 mAh/g of reversible gravimetric capacity is observed, which shows capacity fade compared to the first charge of 139 mAh/g. The corresponding reversible volumetric capacity for the first charge is 692 Ah/L. This is significantly greater than the volumetric capacity of the sodiation of hard carbon and is also similar to the lithiation volumetric capacity of graphite in a lithium ion cell. The capacity faded significantly by cycle 30 and coulombic efficiency was poor as shown in

Figure 5(b). However little capacity fade was observed after cycle 30, when the polarization had become low. During the 50th cycle the polarization decreased by almost a factor of two, to about 438 mV. This low polarization is atypical of a conversion reaction and is more suggestive of intercalation. Apparently a material with good cycling characteristics and low polarization was formed during cycling. Nevertheless, cycling performance would still have to be improved for this material to have practical application. Figure 6(a) shows the voltage curve for 2nd cycle of $Ca_5Co_4(VO_4)_6$ vs. Na. This material has an attractive average voltage of about 0.60 V vs. Na and a reversible volumetric capacity is 625 Ah/L, again considerably exceeding the volumetric capacity of the sodiation of hard carbon. During the 50th cycle the polarization increases by a factor of two, to about 1.04 V. Also the capacity fades significantly, as shown in Figure 6(b). Clearly, compared to $CoTiO_3$, $Ca_5Co_4(VO_4)_6$ undergoes a different sodiation mechanism. Again, cycling performance would have to be improved for this material to have practical application.

Ex-situ X-ray diffraction of fully sodiated materials –

Ex-situ XRD patterns of fully sodiated $CoTiO_3$, $Ca_5Co_4(VO_4)_6$ and CoV_3O_8 are shown in Figure 7.

215 **Figure 5(a)**

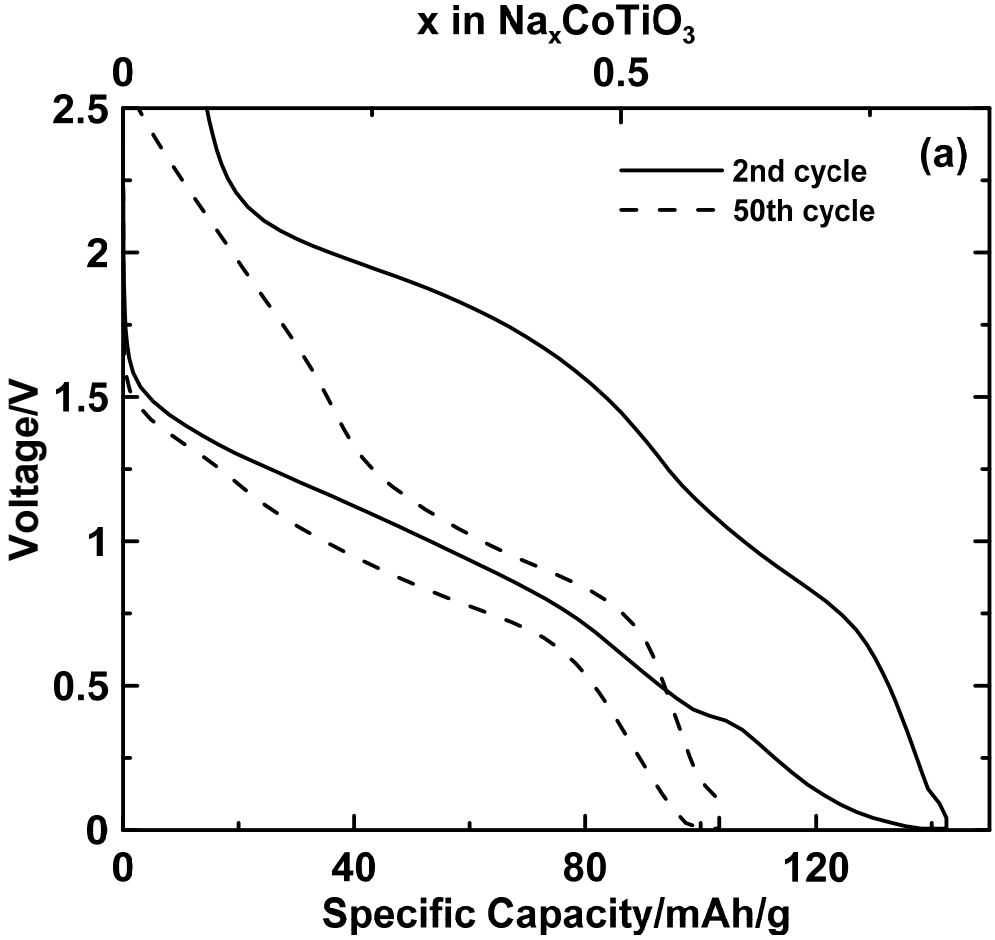

216
217

Figure 5(b)

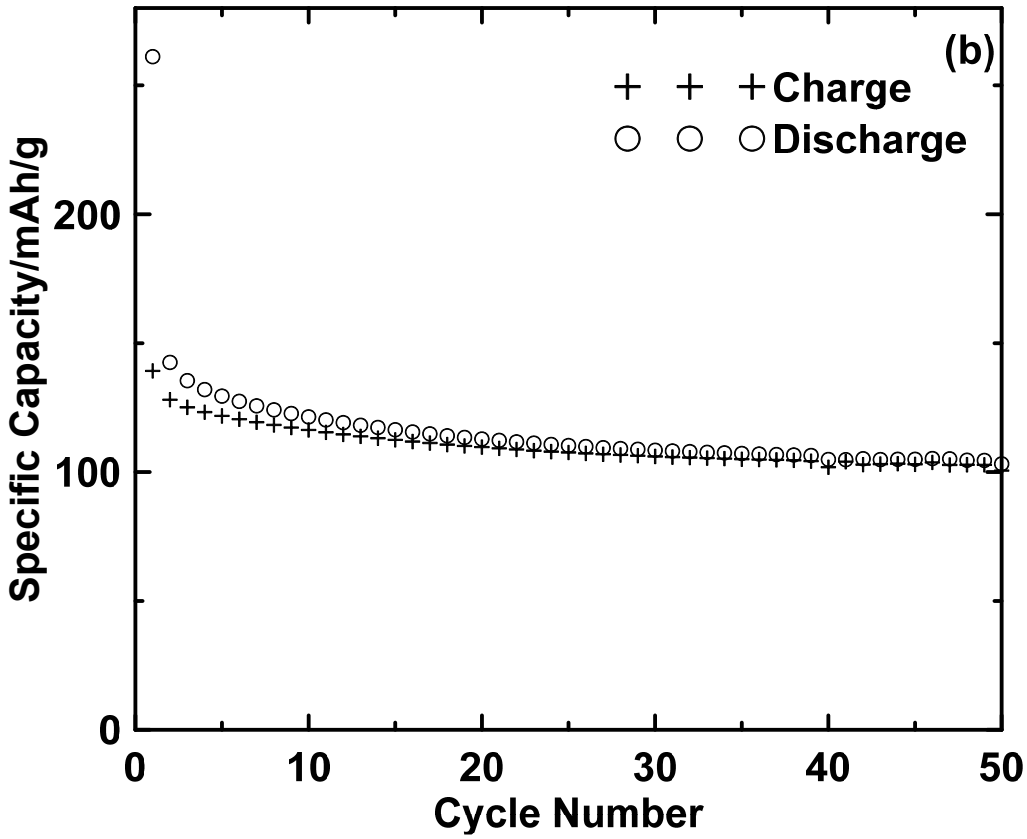
(b)
Charge
Discharge
Specific Capacity/mAh/g
0
100
200
0
10
20
30
40
50
Cycle Number

222 **Figure 6(a)**

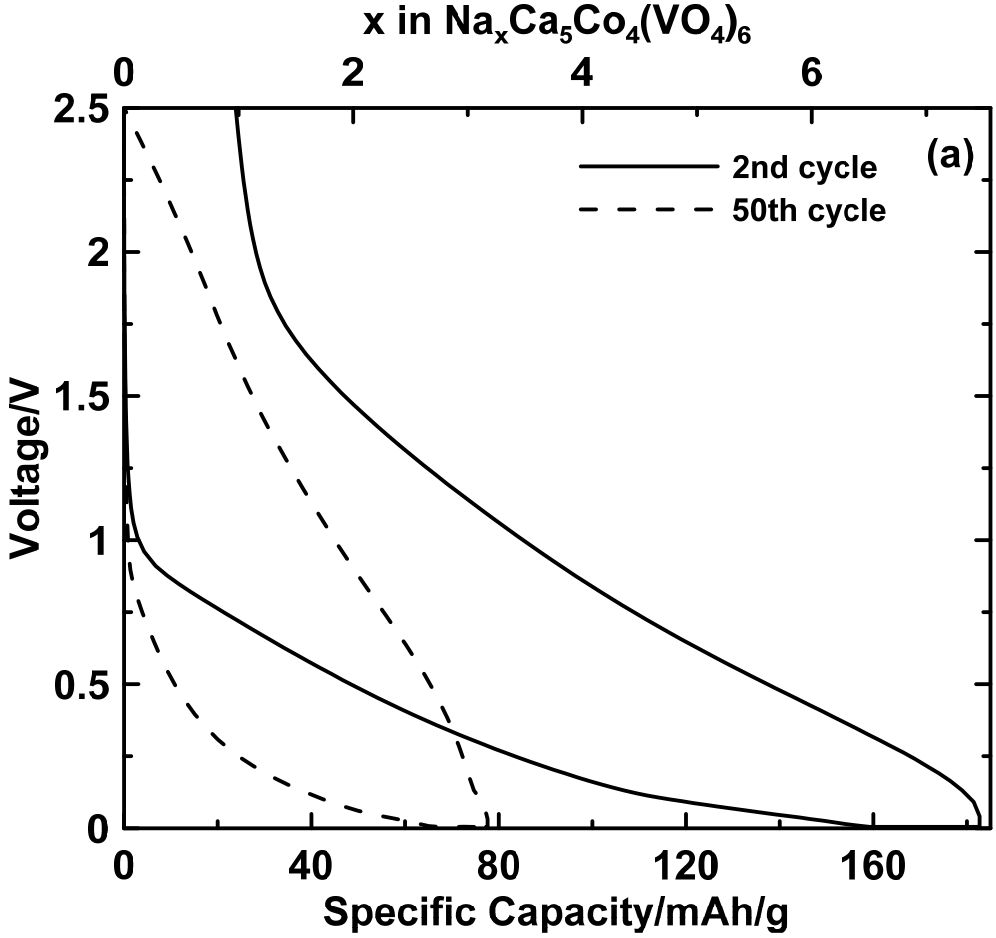

223
224

225 **Figure 6(b)**
226

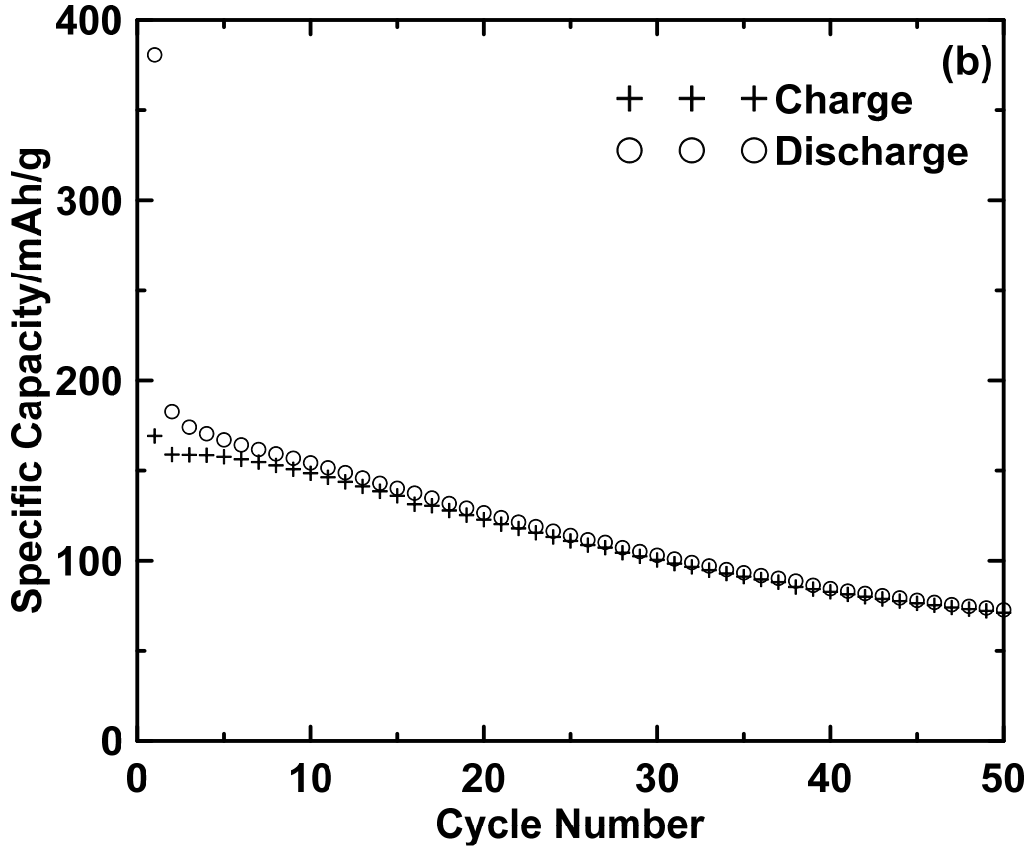

227
228

The sharp peak below 20° as well as the broad peaks at about 44° are artifacts from the XRD sample holder (indicated by + in Figure 7). Other sharp peaks observed in the patterns correspond to unreacted precursors (indicated by ♦ in Figure 7), however these are small in area. All patterns demonstrate drastic amorphization with upon sodiation, which is remarkable, given that only a fraction of the theoretical capacity is accessed. For each of these oxides, this indicates that the entire material has taken part in the sodiation reaction, resulting in the destruction of the original structure. The low capacity of these materials compared to a full conversion reaction coupled with their reacting in their entirety during discharge, suggests a mechanism other than conversion is taking place. As mentioned in the introduction, complex reduction reactions involving oxygen reduction are well known to occur during the lithiation of vanadates.[15,16,18] Such mechanisms may also be occurring here. The development of a broad peak at approximately 41° is observed for sodiated $CoTiO_3$, which prompted further investigation in to its sodiation mechanism, and will be discussed below.

Volume expansion of sodiated $CoTiO_3$ – The thickness of four $CoTiO_3$ electrodes were measured before and after sodiation to determine volume expansion. The average initial coating thickness was 42 ± 2 μm. This corresponds to an average electrode porosity of 50%, which is a typical value for an uncalendered coating.[21] The average final coating thickness was 44 ± 2 μm. If the percent coating porosity is assumed to be constant during sodiation (as it is during the expansion of alloy coatings in lithium cells[21]), this corresponds to a surprisingly low volume expansion of only 6%. This low volume expansion is further evidence of an intercalation-type mechanism, and may explain the relatively good cycling observed for $CoTiO_3$.

Quasi in-situ X-ray diffraction of $CoTiO_3$ vs. Na - Figure 8 shows XRD patterns that were measured at open circuit at different points along the voltage curve of a $CoTiO_3$ vs. Na cell fitted with a Be window. The cell voltage curve is also shown, so that the XRD patterns can be correlated to the points in the voltage curve at which they were measured. Peaks consistently present for all XRD patterns are attributed to BeO and cell parts. During the first discharge, $CoTiO_3$ is consumed and a broad peak at approximately 41° appears as $CoTiO_3$ is sodiated. Subsequently, this broad peak disappears as the material is desodiated during the first charge. Furthermore, crystalline $CoTiO_3$ does not appear to be regenerated after charging. During the second discharge the broad peak at approximately 41° reappears as the material is sodiated. It is possible that the broad peak at approximately 41° can be attributed to the main peak of $NaTiO_2$ with the R-3m (166) space group (PDF# 00-089-0802). If this were the case, then, the following reaction can be proposed:

$$CoTiO_3 + Na \rightleftharpoons NaTiO_2 + CoO. \quad (2)$$

The theoretical capacity of this reaction is 173 mAh/g which is comparable to the observed reversible capacity of 139 mAh/g. This reaction would suggest a three phase mechanism is occurring. Recently, a three phase separation mechanism has been confirmed for the sodiation of $Li_4Ti_5O_{12}$.[22] Similar to the above mechanism, new phases that were formed were not distinguishable until near the end of discharge for the sodiation of $Li_4Ti_5O_{12}$, likely due to the sluggish nucleation and growth of new phases from slow Na^+ kinetics.[22] This supports the possibility of the suggested $CoTiO_3$/Na mechanism, however, a CoO phase was not observed and therefore more evidence is required. Given these materials decompose to the amorphous state, Mössbauer (of Fe containing oxides) and NMR studies may provide further understanding.

Conclusions

Several mixed transition metal titanates and vanadates were synthesized and electrochemically investigated as anode materials in Na and Li cells. Most of these materials had significantly higher lithiation capacity than sodiation capacity, however all capacities were much lower than those for a full conversion reaction. Of these materials, $CoTiO_3$, $VFeO_4$, $Ca_5Co_4(VO_4)_6$, CoV_3O_8, and MnV_2O_6 exhibited significant volumetric capacities with sodium between 0.005 – 2.5 V. The volumetric capacities of these materials are much greater than the sodiation of hard carbon and, in some cases, greater than that for the lithiation of graphite. Fully discharged $CoTiO_3$, $Ca_5Co_4(VO_4)_6$, and CoV_3O_8 in Na cells were found to be amorphous even though their capacity is only a small fraction of what would be predicted for a full conversion type reaction. This suggests a mechanism other than conversion is occurring.

$CoTiO_3$ was found to have particularly interesting characteristics as an anode in Na cells. After 30 cycles the voltage curve polarization of $CoTiO_3$ reduced to only 438 mV. The volume expansion during sodiation was measured to be only 6%. Both the low polarization and low volume expansion are suggestive of an intercalation type mechanism. If such oxides could be made with low irreversible capacity they would be attractive for use as high volumetric capacity anodes in Na-ion cells.

Acknowledgements

The authors thank the Natural Sciences and Engineering Research Council of Canada (NSERC) and 3M Company for funding. We also acknowledge the support of the Canada Foundation for

Innovation, the Atlantic Innovation Fund and other partners that fund the Facilities for Materials Characterization managed by the Institute for Research in Materials.

References

1. M. Armand and J.-M. Tarascon, *Nature*, **451**, 652–7 (2008).

2. S.-W. Kim, D.-H. Seo, X. Ma, G. Ceder, and K. Kang, *Adv. Energy Mater.*, **2**, 710–721 (2012).

3. B. L. Ellis and L. F. Nazar, *Curr. Opin. Solid State Mater. Sci.*, **16**, 168–177 (2012).

4. D. P. DiVincenzo and E. J. Mele, *Phys. Rev. B*, **32**, 2538 (1985).

5. D. A. Stevens and J. R. Dahn, *J. Electrochem. Soc.*, **147**, 1271 (2000).

6. P. Senguttuvan, M. R. Palacín, G. Rousse, V. Seznec, and J.-M. Tarascon, *Chem. Mater.*, **23**, 4109–4111 (2011).

7. R. Shanmugam and W. Lai, *ECS Electrochem. Lett.*, **3**, A23–A25 (2014).

8. R. Fielden and M. N. Obrovac, *J. Electrochem. Soc.*, **161**, A1158–A1163 (2014).

9. R. Malini, U. Uma, T. Sheela, M. Ganesan, and N. G. Renganathan, *Ionics (Kiel).*, **15**, 301–307 (2008).

10. F. Klein, B. Jache, A. Bhide, and P. Adelhelm, *Phys. Chem. Chem. Phys.*, **15**, 15876–87 (2013).

11. J. L. Tirado, *Mater. Sci. Eng. R Reports*, **40**, 103 (2003).

12. R. Alcantara, M. Jaraba, P. Lavela, and J. L. Tirado, *Chem. Mater.*, **14**, 2847–2848 (2002).

13. Y. Jiang, M. Hu, D. Zhang, T. Yuan, W. Sun, B. Xu and M. Yan, *Nano Energy*, **5**, 60–66 (2014).

14. S. Denis, E. Baudrin, M. Touboul, and J.-M. Tarascon, *J. Electrochem. Soc.*, **144**, 4099 (1997).

15. E. Baudrin, S. Laruelle, S. Denis, M. Touboul, and J. Tarascon, *Solid State Ionics*, **123**, 139–153 (1999).

16. S. Kim, H. Ikuta, and M. Wakihara, *Solid State Ionics*, **139**, 57–65 (2001).

17. S. Denis, E. Baudrin, F. Orsini, G. Ouvrard, M. Touboul and J.-M.Tarascon, *J. Power Sources*, **81-82**, 79–84 (1999).

18. S. Denis, E. Baudrin, M. Touboul, and J.-M. Tarascon, *J. Electrochem. Soc.*, **144**, 4099 (1997).

19. K. Periyapperuma, T. T. Tran, S. Trussler, D. Iaboni, and M. N. Obrovac, *To be Submitt. (n. d.)*.

20. International Centre for Diffraction Data, *PDF-2* (2002).

21. Z. Du, R. A. Dunlap, and M. N. Obrovac, *To be Submitt. (n. d.)*.

22. Y. Sun, L. Zhao, H. Pan, X. Lu, L. Gu, Y.-S. Hu, H. Li, M. Armand, Y. Ikuhara, L. Chen and X. Huang., *Nat. Commun.*, **4**, 1870 (2013).

337 **Table 1**. Milling/heating conditions for the preparation of materials.

End Product	Precursors	Milling Conditions	Heating Conditions
$CoTiO_3$ (ilmenite structure)	Co_3O_4 (<10μm, Sigma-Aldrich) TiO_2 (puriss, 99 – 100.5 %, Sigma-Aldrich)	Two hours in air	800°C for 10 hours in air
$MnTiO_3$ (ilmenite structure)	MnO_2 (60 - 230 mesh, > 99%, Sigma-Aldrich) TiO_2 (puriss, 99 – 100.5 %, Sigma-Aldrich)	One hour in air	1100°C for 10 hours in argon
$VFeO_4$ (triclinic $VFeO_4$ structure)	V_2O_5 (> 99.6%, Sigma-Aldrich) Fe_2O_3 (< 5 μm, > 99%, Sigma-Aldrich)	One hour in air	550°C for 24 hours in air
$Ca_5Co_4(VO_4)_6$ (cubic $Ca_5Co_4(VO_4)_6$ structure)	CaO (99.9%, Sigma-Aldrich) CoO (-325 mesh, Sigma-Aldrich) V_2O_5 (>99.6%, Sigma-Aldrich)	One hour in argon	750°C for 10 hours in argon
$Co_2V_2O_7$ (dichromate structure)	Co_3O_4 (<10 μm, Sigma-Aldrich) V_2O_5 (> 99.6%, Sigma-Aldrich)	One hour in air	600°C for 30 hours in air
CoV_3O_8 (orthorhombic α-CoV_3O_8 structure)	CoO (-325 mesh, Sigma-Aldrich) V_2O_4 (99.9% trace metals basis) V_2O_5 (> 99.6%, Sigma-Aldrich)	One hour in argon	600°C for 12 hours in argon
$Mn_2V_2O_7$ (thortveitite structure)	MnO (-60 mesh, 99%, Sigma-Aldrich) and V_2O_5 (> 99.6%, Sigma-Aldrich)	One hour in air	600°C for 30 hours in air
MnV_2O_6 (brannerite structure)	Mn_2O_3 (-325 mesh, 99%, Sigma-Aldrich) V_2O_5 (> 99.6%, Sigma-Aldrich	One hour in air	800°C for 30 hours in air
$CrVO_4$ (orthorhombic β-$CrPO_4$ structure)	Cr_2O_3 (50 μm, > 98%, Sigma-Aldrich) V_2O_5 (> 99.6%, Sigma-Aldrich)	One hour in air	800°C for 30 hours in air
$TiVO_4$ (pseudo rutile structure)	TiO_2 (puriss, 99 – 100.5 %, Sigma-Aldrich) V_2O_5 (> 99.6%, Sigma-Aldrich)	30 minutes in argon	1000°C for 16 hours in argon

338

339

340 **Table 2**. Crystallographic densities, and reversible specific and volumetric capacities between 0
341 V and 2.5 V in Li and Na cells of the mixed metal oxides studied here.

342

Material	Density / (g/cm^3)	Reversible Specific Capacity vs. Li / (mAh/g)	Reversible Volumetric Capacity vs. Li /(Ah/L)	Reversible Specific Capacity vs. Na / (mAh/g)	Reversible Volumetric Capacity vs. Na / (Ah/L)
$CoTiO_3$	4.98	167	832	139	692
$MnTiO_3$	4.54	-	-	16	73
$VFeO_4$	3.68	1214	5696	316	1163
$Ca_5Co_4(VO_4)_6$	3.70	620	2414	169	625
$Co_2V_2O_7$	4.28	942	4022	62	265
CoV_3O_8	3.8	847	3186	251	953
$Mn_2V_2O_7$	3.79	891	3393	30	114
MnV_2O_6	4.10	712	2855	200	820
$CrVO_4$	4.06	90	358	18	73
$TiVO_4$	4.37	54	236	28	122

343
344

345 Figure Captions

346 **Figure 1.** XRD patterns of all synthesized materials and their matching reference patterns. Black
347 circles indicate the $Co_3V_2O_8$ impurity (PDF# 00-070-1393) phase found with $Ca_5Co_4(VO_4)_6$.

348 **Figure 2.** Observed reversible capacities of all materials studied vs. Li (dashed line) and Na
349 (solid line) with the theoretical capacity plotted as a red vertical line.

350 **Figure 3.** The observed reversible capacity vs. theoretical capacity for Li cells (diamond) and Na
351 cells (circle) of all materials. A line indicating when the observed capacity is equal to the
352 theoretical capacity is shown for comparison.

353 **Figure 4.** Polarization between the first charge and second discharge for Li cells and Na cells of
354 the materials studied with significant capacity below 2.5 V.

355 **Figure 5.** Voltage curves for the 2^{nd} and 50^{th} cycle (a) and the cycling performance (b) of
356 $CoTiO_3$ vs. Na.

357 **Figure 6.** Voltage curves for the 2^{nd} and 50^{th} cycle (a) and the cycling performance (b) of
358 $Ca_5Co_4(VO_4)_6$ vs. Na.

359 **Figure 7**. *Ex-situ* powder X-ray diffraction patterns for sodiated $CoTiO_3$, $Ca_5Co_4(VO_4)_6$, and
360 CoV_3O_8. Artifacts from the air sensitive holder (+) and peaks of unreacted precursors (♦) are
361 labelled.

362 **Figure 8.** Quasi *in-situ* investigation of $CoTiO_3$/Na cell. The voltage vs. time curve on the right
363 hand side indicates the voltages at which an X-ray pattern was collected. The main peaks for
364 $CoTiO_3$ (dashed line) and $NaTiO_2$ (solid line) are shown below the experimental patterns.

365

Figure 1

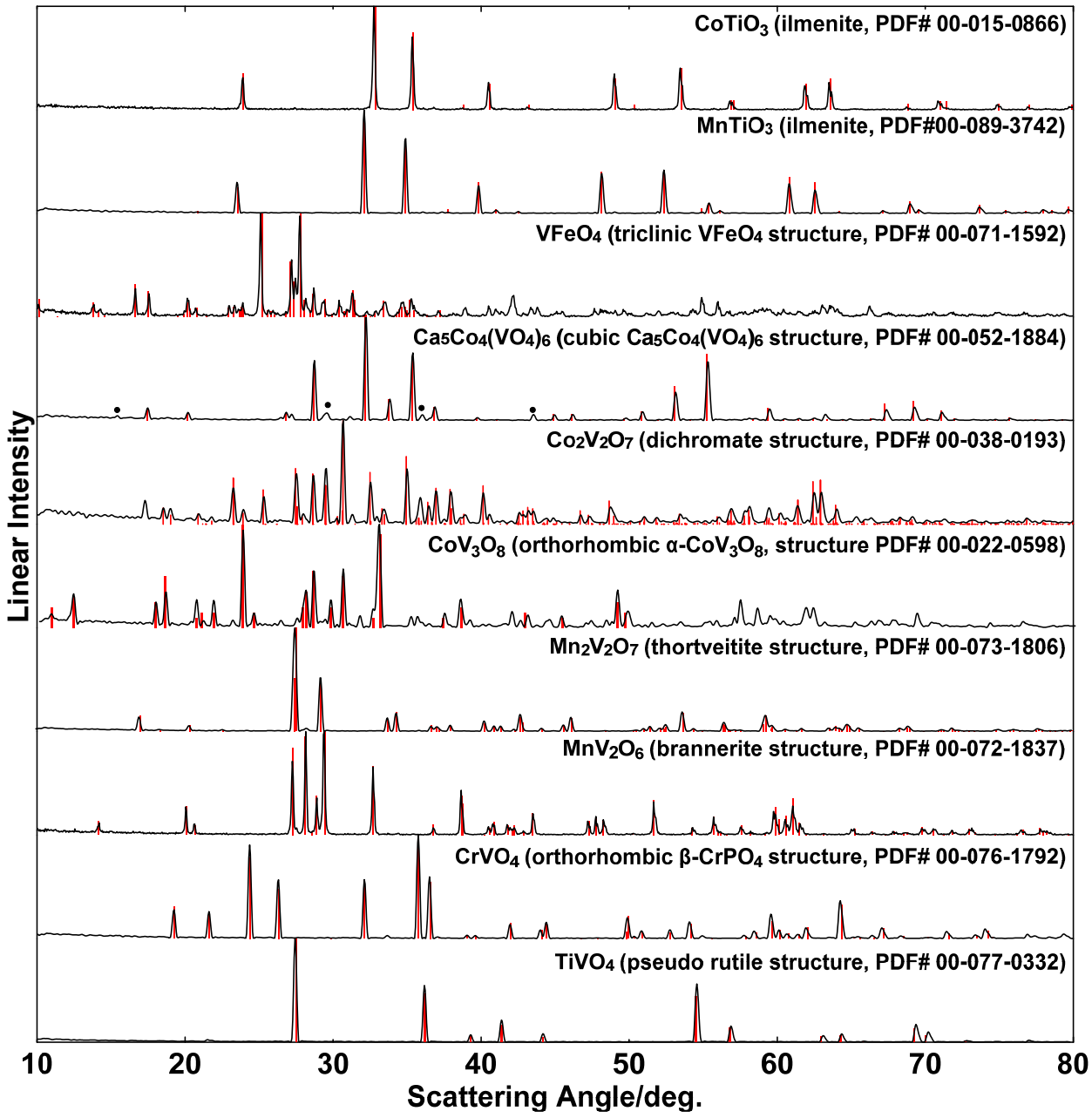
CoTiO3 (ilmenite, PDF# 00-015-0866)
MnTiO3 (ilmenite, PDF#00-089-3742)
VFeO4 (triclinic VFeO4 structure, PDF# 00-071-1592)
Ca5Co4(VO4)6 (cubic Ca5Co4(VO4)6 structure, PDF# 00-052-1884)
Co2V2O7 (dichromate structure, PDF# 00-038-0193)
CoV3O8 (orthorhombic α-CoV3O8, structure PDF# 00-022-0598)
Mn2V2O7 (thortveitite structure, PDF# 00-073-1806)
MnV2O6 (brannerite structure, PDF# 00-072-1837)
CrVO4 (orthorhombic β-CrPO4 structure, PDF# 00-076-1792)
TiVO4 (pseudo rutile structure, PDF# 00-077-0332)
Linear Intensity
10
20
30
40
50
60
70
80
Scattering Angle/deg.

371 **Figure 2**

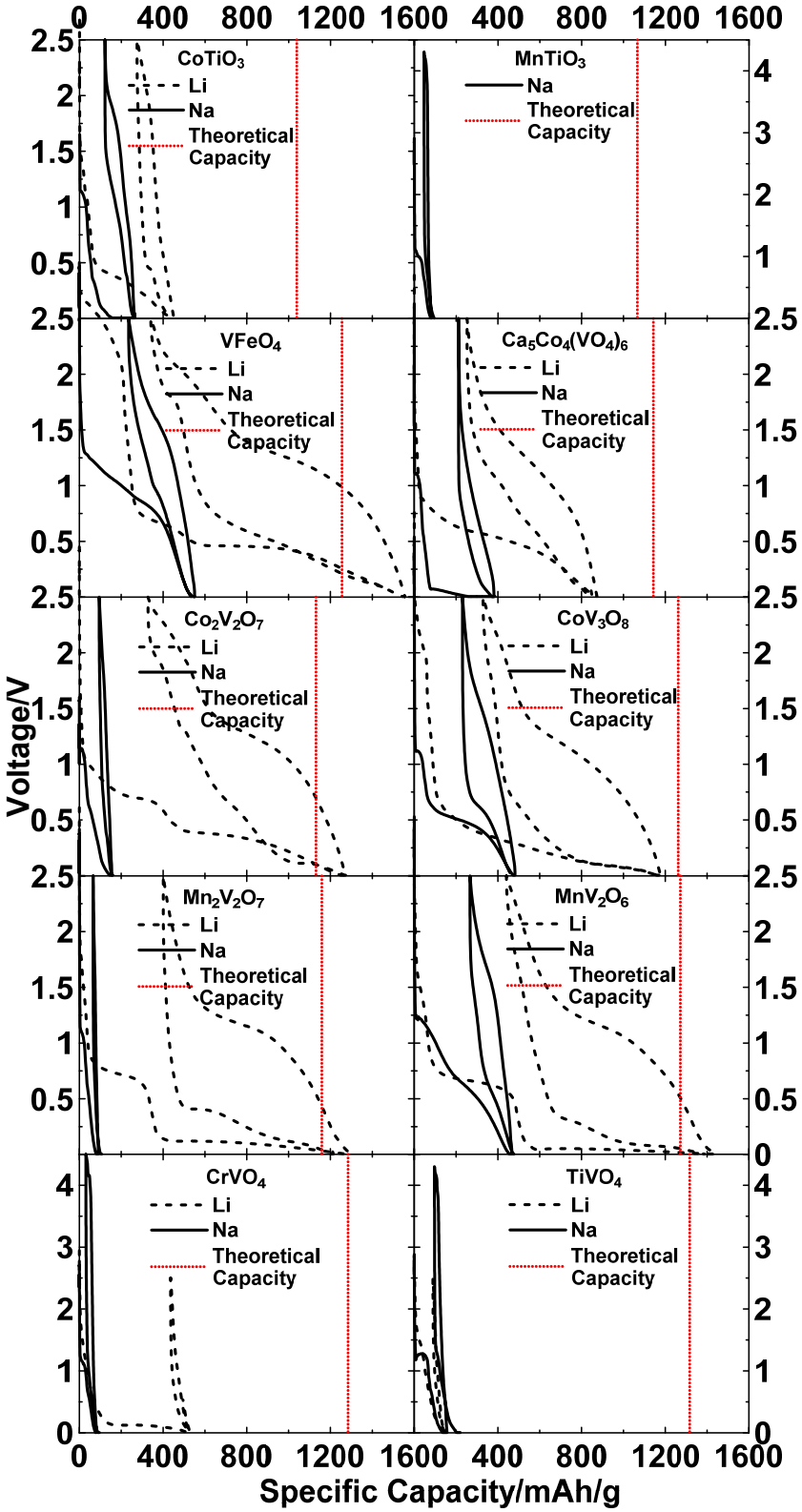

372
373

374 **Figure 3**

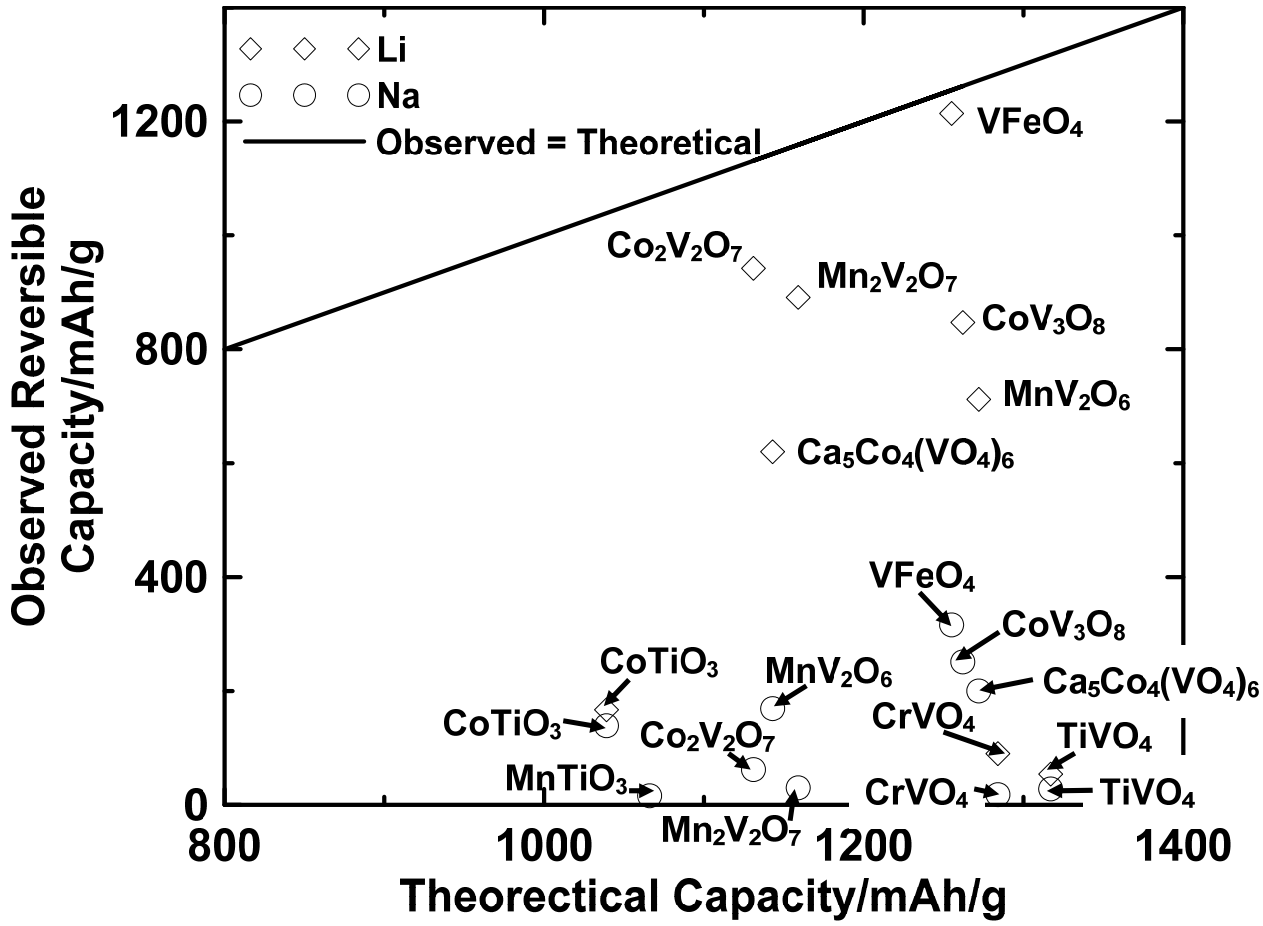

375

376

377 **Figure 4**

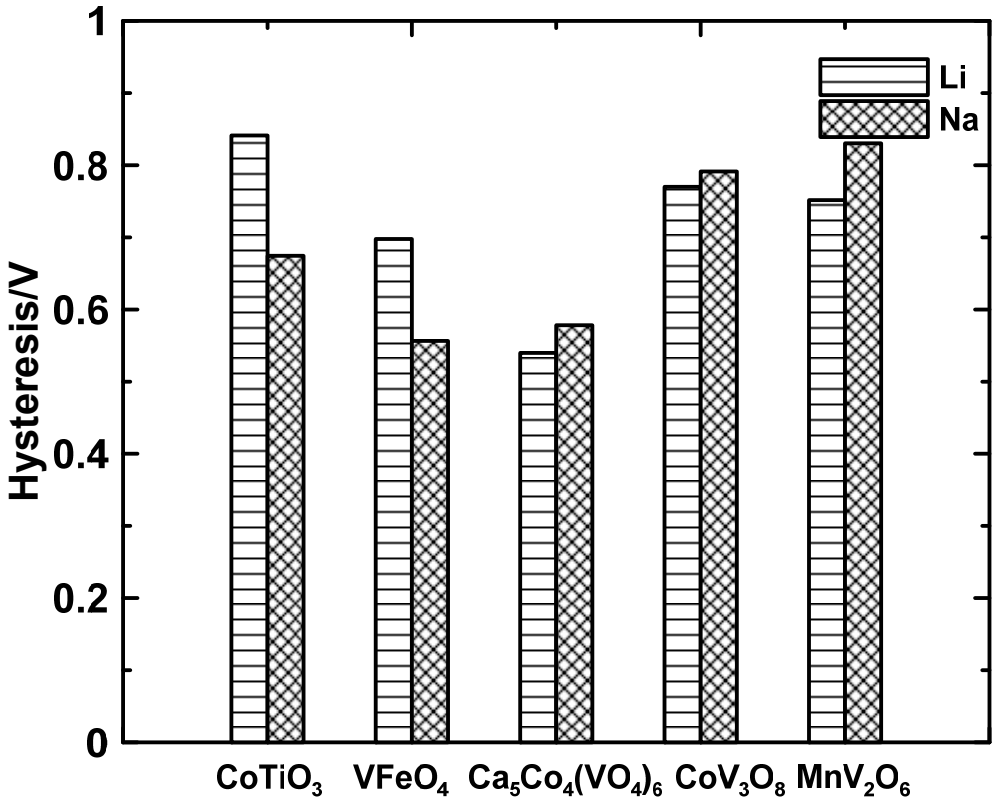

378

379

380 **Figure 5(a)**

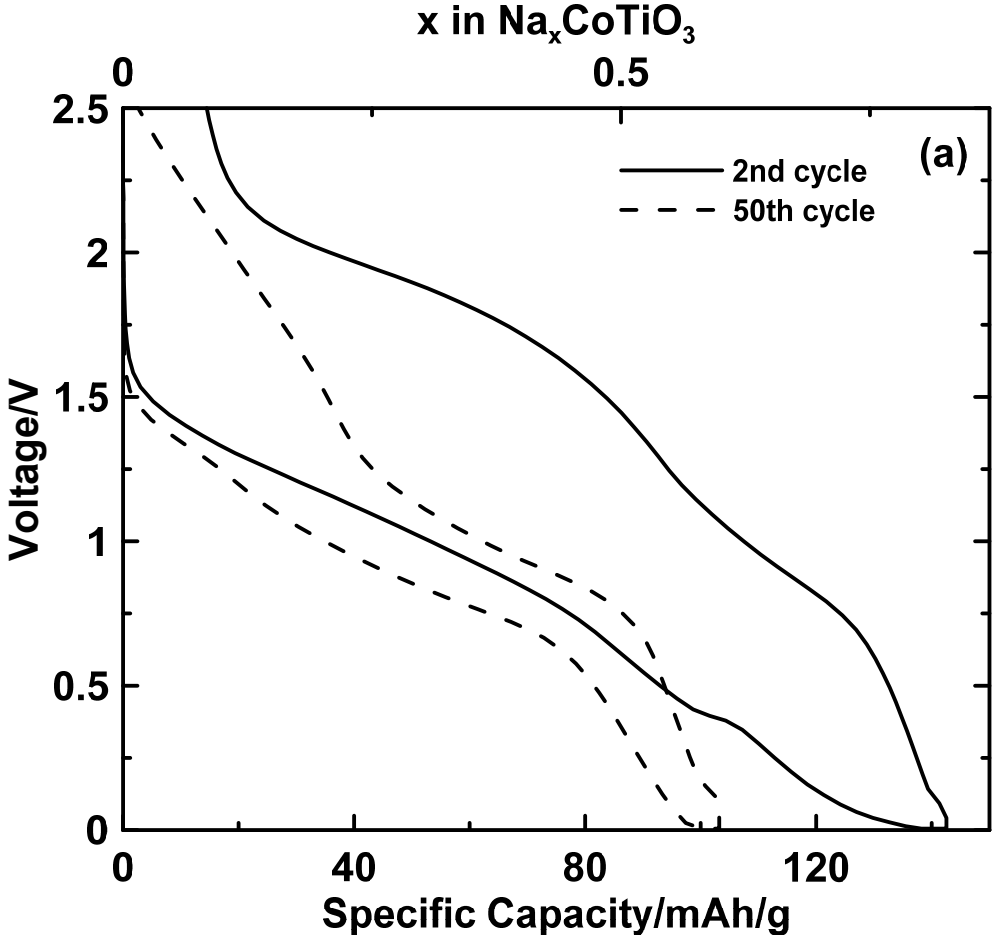

381
382

Figure 5(b)

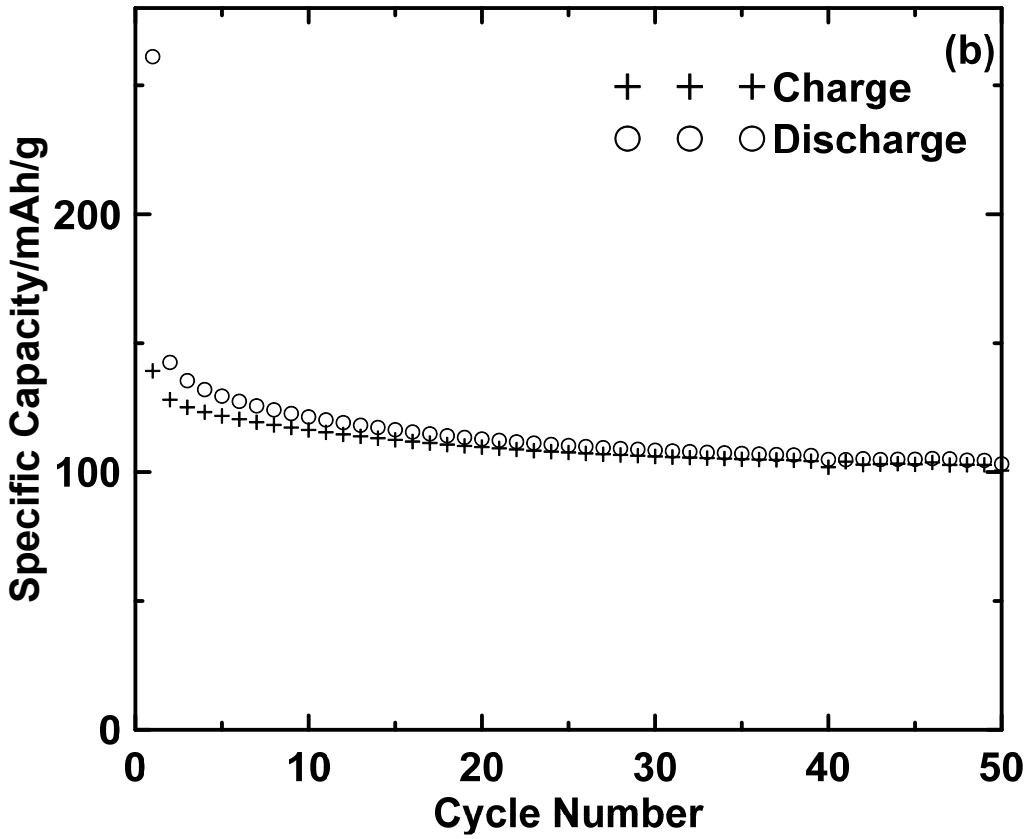
(b)
Charge
Discharge
Specific Capacity/mAh/g
0
100
200
0
10
20
30
40
50
Cycle Number

387 **Figure 6(a)**

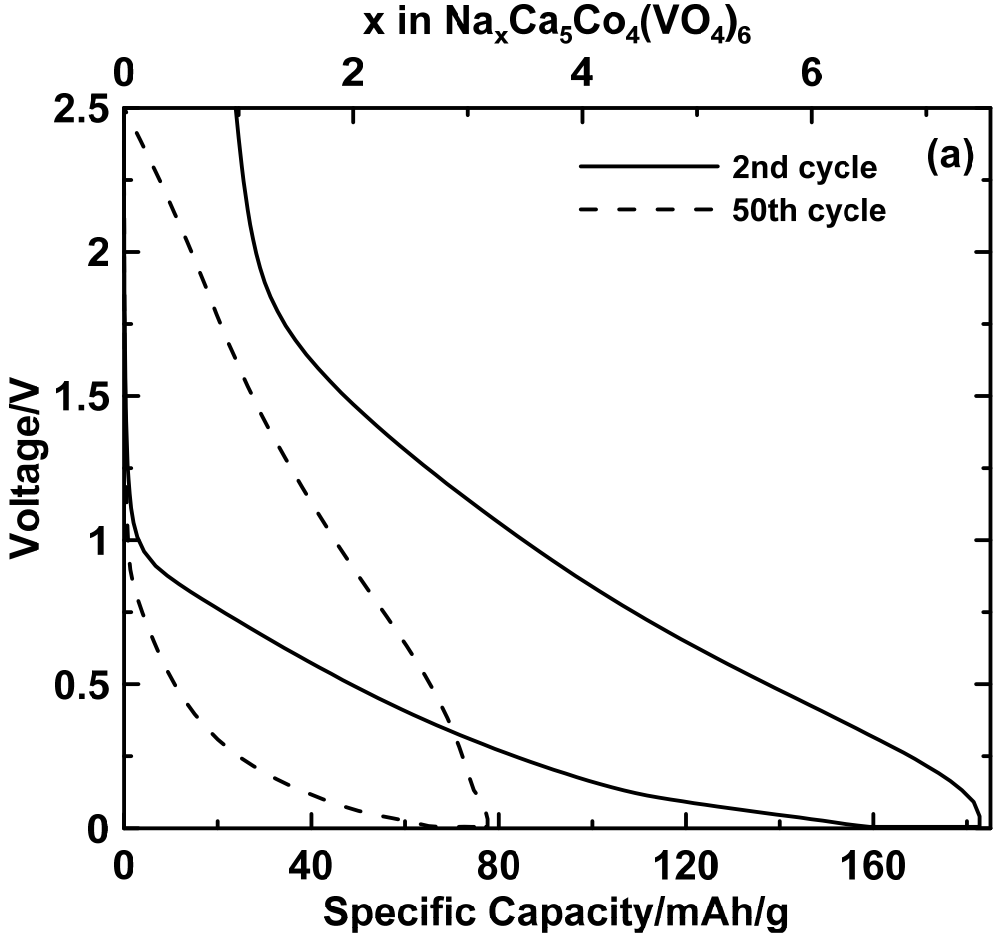

388
389

Figure 6(b)

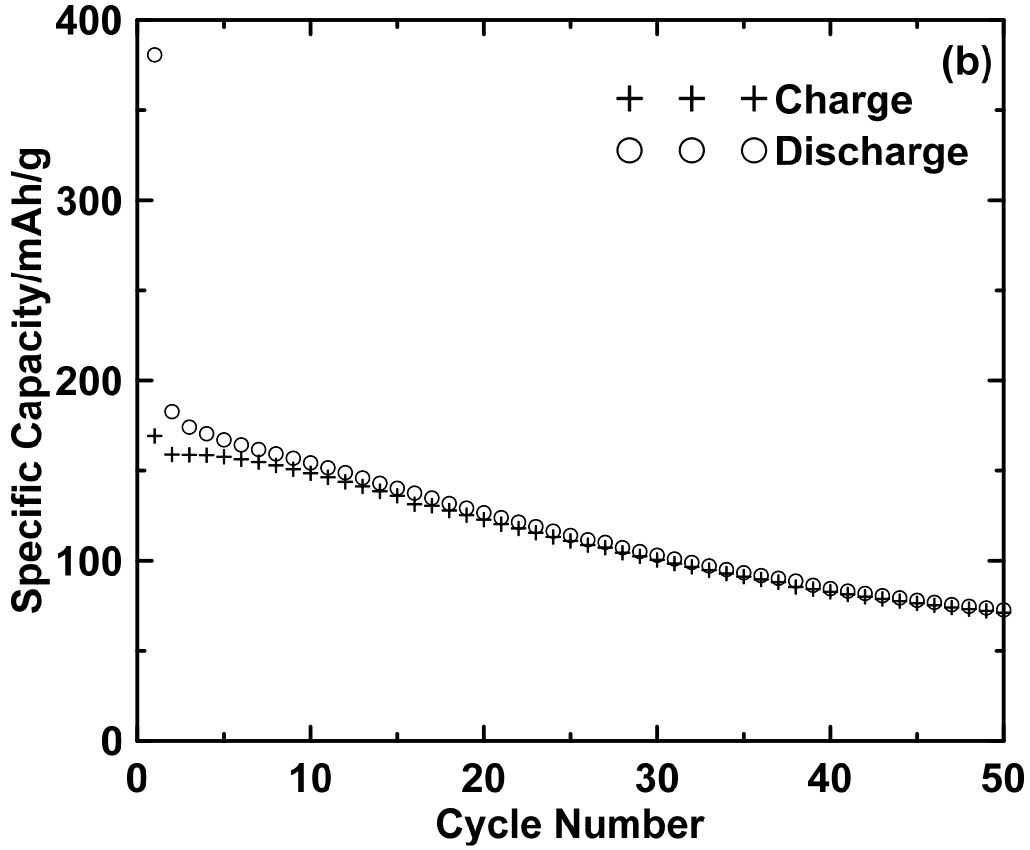
(b)
Charge
Discharge
Specific Capacity/mAh/g
Cycle Number
0
100
200
300
400
0
10
20
30
40
50

394 **Figure 7**

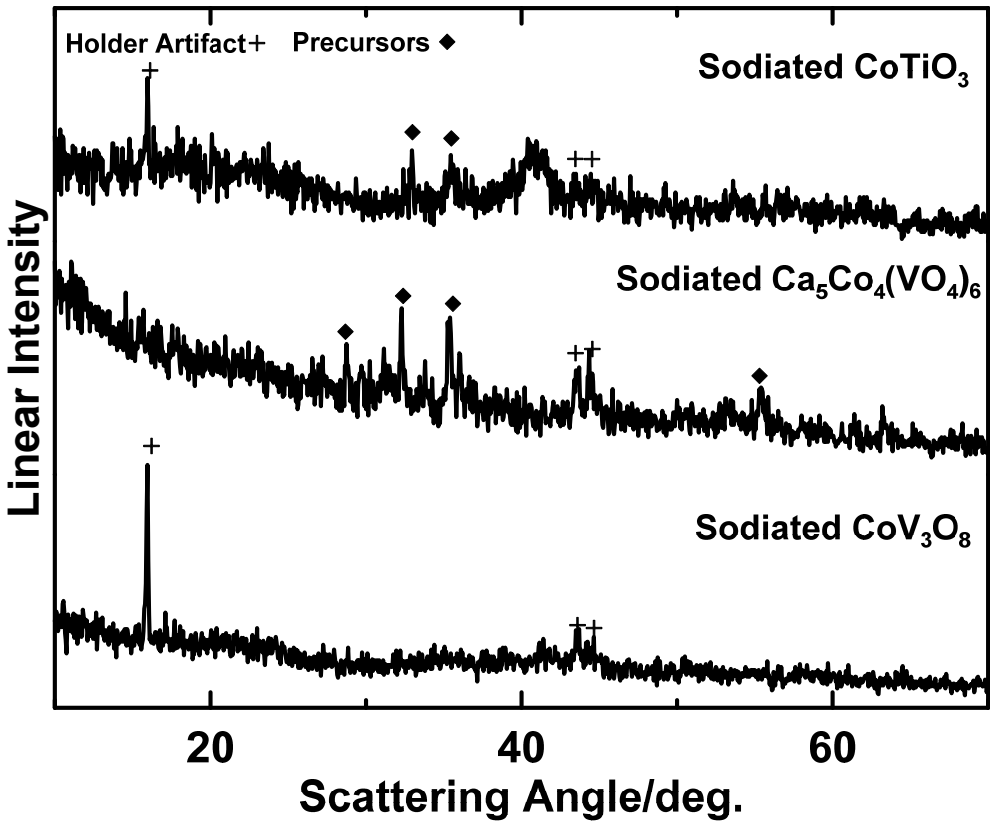

395

396

397 **Figure 8**

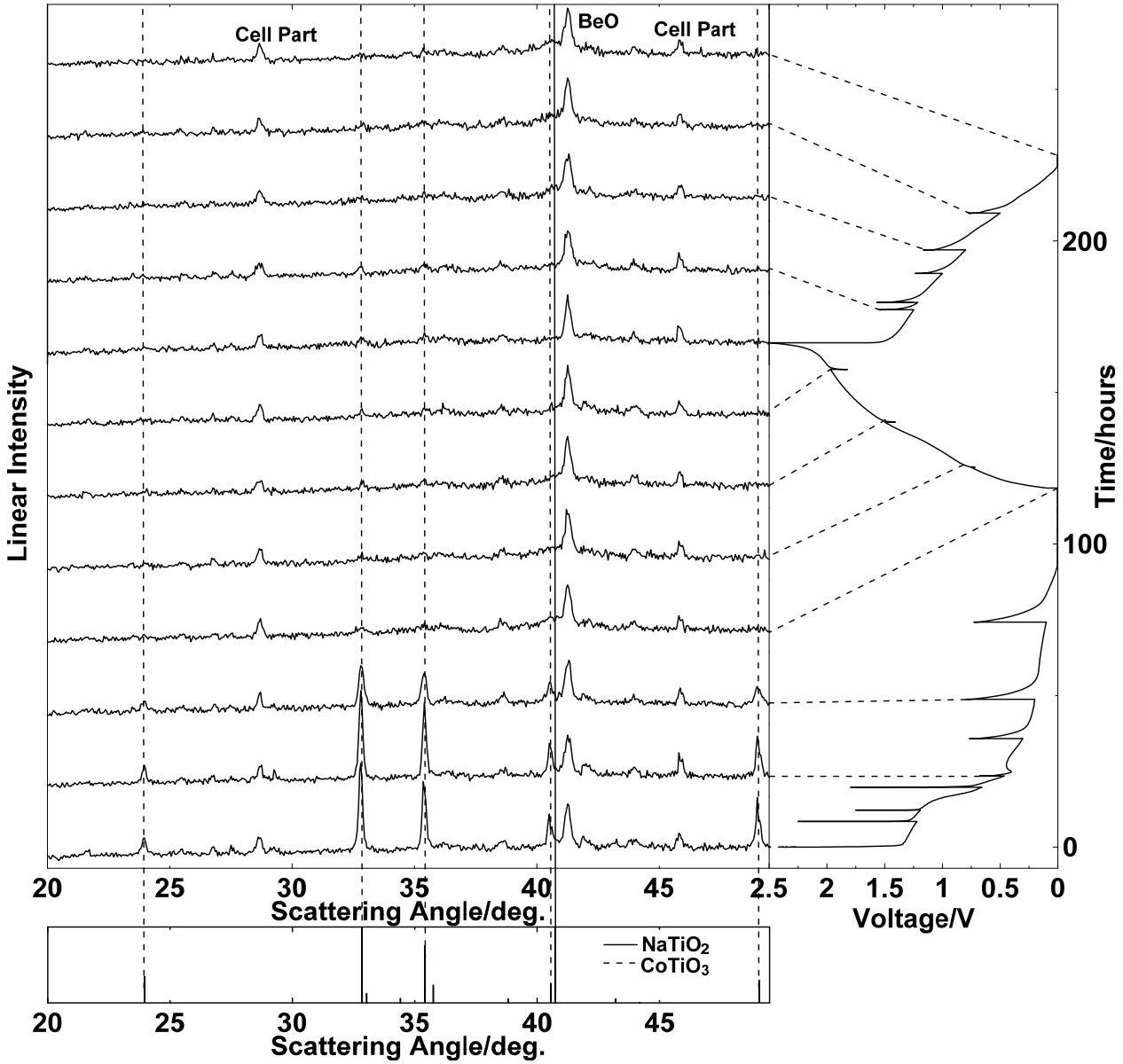

398